PNAS RESEARCH ARTICLE | ENVIRONMENTAL SCIENCES ANTHROPOLOGY

# Nile waterscapes facilitated the construction of the Giza pyramids during the 3rd millennium BCE

Hader Sheisha[a,b,1], David Kaniewski[c,d], Nick Marriner[e], Morteza Djamali[b], Gamal Younes[a,f], Zhongyuan Chen[g], Gad El-Qady[h], Amr Saleem[f], Alain Véron[a], and Christophe Morhange[a,i]

Edited by Linda Manzanilla, Universidad Nacional Autonóma de México, Mexico, D.F., Mexico; received February 13, 2022; accepted June 29, 2022

**The pyramids of Giza originally overlooked a now defunct arm of the Nile. This fluvial channel, the Khufu branch, enabled navigation to the Pyramid Harbor complex but its precise environmental history is unclear. To fill this knowledge gap, we use pollen-derived vegetation patterns to reconstruct 8,000 y of fluvial variations on the Giza floodplain. After a high-stand level concomitant with the African Humid Period, our results show that Giza's waterscapes responded to a gradual insolation-driven aridification of East Africa, with the lowest Nile levels recorded at the end of the Dynastic Period. The Khufu branch remained at a high-water level (∼40% of its Holocene maximum) during the reigns of Khufu, Khafre, and Menkaure, facilitating the transportation of construction materials to the Giza Pyramid Complex.**

Great pyramid | Nile | Giza Harbour

## Significance

The pyramids of Giza constitute one of the world's most iconic cultural landscapes and have fascinated humanity for thousands of years. Indeed, the Great Pyramid of Giza (Khufu Pyramid) was one of the Seven Wonders of the Ancient World. It is now accepted that ancient Egyptian engineers exploited a former channel of the Nile to transport building materials and provisions to the Giza plateau. However, there is a paucity of environmental evidence regarding when, where, and how these ancient landscapes evolved. New palaeoecological analyses have helped to reconstruct an 8,000-year fluvial history of the Nile in this area, showing that the former waterscapes and higher river levels around 4,500 years ago facilitated the construction of the Giza Pyramid Complex.

The Nile River, with its dynamic floods and migratory behavior, played a key role in shaping ancient Egyptian history (1). The pyramids of Khufu, Khafre, and Menkaure, located on the Giza Plateau, overlook the west bank of the Nile (Egypt). Built during the Fourth Dynasty (Old Kingdom 2686–2160 BCE) (2), they are one of the world's most iconic cultural landscapes and constitute ancient engineering feats that have fascinated humanity for millennia. To edify the plateau's pyramids, tombs, and temples, it now seems that ancient Egyptian engineers took advantage of the Nile and its annual floods (3, 4), using an ingenious system of canals and basins that formed a port complex at the foot of the Giza plateau (5, 6). The harbor complex currently lies >7 km west of the present-day Nile, but it is widely accepted that Fourth Dynasty engineers exploited a now defunct branch of the Nile (7), which flowed along the western edge of the Nile floodplain during the Egyptian Old Kingdom and that we refer to as the Khufu branch. These canals and basins had to be deep enough to accommodate shallow-draft vessels all year round. Larger cargo ships could probably only navigate during the flood season (August–October), when water levels in the Nile channel rose by ∼7 m (8, 9).

The existence of a paleo-channel, canals, and harbors is now supported by recent archaeological findings (5, 6), as well as research related to the "Lost City of the Pyramids" (the Heit el-Ghurab site) (7, 10, 11). Core drillings and subterranean engineering works for Giza's modern urban projects have yielded stratigraphic evidence consistent with a paleo-branch of the Nile. In particular, Old Kingdom structures unearthed during these interventions offer insights into the local cultural waterscape at the time of the pyramid builders. Furthermore, the Wadi el-Jarf Papyri, discovered at a Khufu-age port on the Red Sea coast (9, 12, 13), attest to the existence of such a harbor complex, called Ro-She Khufu ("Entrance to the Lake…" or "…Basin of Khufu"). The *Journal of Merer*, a large corpus of these papyri, describes the transport of limestone from Toura, ∼17 km from the Giza Plateau, to the construction site of the Great Pyramid of Khufu. A striking parallel exists between the names of the basins and waterways in the papyri and the spatial organization of Giza's Fourth Dynasty waterscape, as reconstructed by archaeologists (5).

The fluvial-port-complex hypothesis postulates that pyramid builders cut through the western levee of the Khufu branch of the Nile and dredged basins down to river depth in order to harness the annual 7-m rise of the flood like a hydraulic lift, bringing the higher water levels to the base of the Giza plateau (5, 6). In this way, it was possible to transport supplies and building materials directly to the pyramid complex. These canals and ports would also have been key for the longer-distance transport of materials via the Nile, facilitating transport logistics and for the continuous supply of the plateau's diverse building projects and linking Giza with nearby cities in the Memphite region and on the delta. Nonetheless, the interactions between ancient Egyptian societies and environmental changes along the Khufu branch are complex and poorly

Author contributions: H.S., D.K., N.M., and C.M. designed research; H.S., D.K., N.M., G.Y., and C.M. performed research; H.S., D.K., N.M., M.D., Z.C., G.E.-Q., A.S., A.V., and C.M. contributed new reagents/analytic tools; H.S., D.K., N.M., M.D., and C.M. analyzed data; and H.S., D.K., N.M., M.D., and C.M. wrote the paper.

The authors declare no competing interest.

This article is a PNAS Direct Submission.



See online for related content such as Commentaries.

[1]To whom correspondence may be addressed. Email: sheisha@cerege.fr.

This article contains supporting information online at http://www.pnas.org/lookup/suppl/doi:10.1073/pnas.2202530119/-/DCSupplemental.

Published August 29, 2022.

understood. We evaluate its water levels during the last 8,000 y, with a particular focus on the Dynastic Period and the Old Kingdom, using sediment cores and long-term ecosystem dynamics. Our data shed light on previous reconstructions because environmental and historical data are more closely coupled; such resolution has never been achieved in this region. Furthermore, our sequence can be extrapolated to upstream and downstream areas of the Egyptian Nile, allowing comparison with other archaeological sites.

To estimate variations in the water level of the Khufu branch, five cores were drilled on the present Giza floodplain, east of the pyramid complex (Fig. 1 and *SI Appendix*, Figs. S1 and S2). Bioindicators (pollen grains) were extracted from cores G1 and G4 (see dataset for full details) situated in what has been geographically defined as the Khufu branch of the Nile (5, 6). We identified 61 taxa (*SI Appendix*, Fig. S3) grouped into seven pollen-derived vegetation patterns (PdVs) based on their ecological affinities (*SI Appendix*, Table S1). Among the defined PdVs, the Cyperaceae (papyrus, sedge; located on the banks of the Nile), tropical Nilotic taxa (pollen carried downstream by the Nile from tropical areas of the watershed), and helophytes reveal the presence of a permanent waterbody on the Giza floodplain (*SI Appendix*, Table S1). The other PdVs (upland terrestrial herbs, date palm-willow, cereals, and ferns) correspond to a more terrestrial influence. We used these PdV time series (the associated dating error is averaged to ±80 y for the whole sequence) to perform a principal component analysis (PCA) (*SI Appendix*, Fig. S4), using PCA-Axis 1 as a proxy for Holocene Khufu-branch levels (Fig. 2). The negative values of PCA-Axis 1 are loaded by plants located on the Nile floodplain while the positive scores are weighted by taxa deriving from beyond the floodplain (*SI Appendix*, Fig. S4). The highest water levels are attested by high abundances of Cyperaceae and helophytes, with a higher input of tropical pollen from the Nile River, while the low levels are framed by an increase in terrestrial taxa (*SI Appendix*, Fig. S5). Nile flow variations, as deduced from the PCA-Axis 1, are correlated with changes in the lithofacies (*SI Appendix*, Fig. S6).

Our score-based reconstruction shows that the water level of the Khufu branch (termed K-1) was higher during the African Humid Period (14, 15), with a local termination estimated at 3550 ± 80 BCE (5500 ± 80 BP) and a later peak recorded at 2950 ± 80 BCE (Fig. 2) after a significant drop at 3450–3250 ± 80 BCE. During this period, it has been shown that conglomerations of predynastic and early dynastic settlements (3550–3250 BCE) existed along the east bank of the Khufu branch and on the floodplain between the paleo-channel and the pyramid plateau (16, 17). We suggest that the environmental attractivity of Giza during the fourth millennium resulted from a decrease in fluvial levels following the end of the African Humid Period (18). The reconstructed higher level of Khufu branch is also supported by Nile Delta sedimentation rates (correlation $R^2 = 0.75$, *SI Appendix*, Fig. S7) (19, 20), is attributed to increased rainfall over Lake Tana (correlation $R^2 = 0.86$, *SI Appendix*, Fig. S7), the source of the Blue Nile (21) and Lake Victoria (correlation $R^2 = 0.84$, *SI Appendix*, Fig. S7), the source of the White Nile (22). Nile flow is mediated by monsoon activity in tropical Africa. The Holocene intensity of the East African Monsoon, as reconstructed at Lake Abiyata (23) and Lake Rutundu (24) in Ethiopia (Fig. 3), is modulated by the north–south movement of the Intertropical Convergence Zone (ITCZ), with higher rainfall levels during the early Holocene consistent with a more northward migration of the monsoon rain belt driven by higher insolation (25). We found that the Khufu branch has recorded the same trend (Fig. 2), with a high-stand level that correlates with greater summer insolation (correlation $R^2 = 0.88$, *SI Appendix*, Fig. S7) and a northward migration of the ITCZ (correlation $R^2 = 0.83$, *SI Appendix*, Fig. S7), which reinforced the intensity of the East African Monsoon (correlation $R^2 = 0.68$, *SI Appendix*, Fig. S7) over the Nile Valley and created higher flow regimes in the

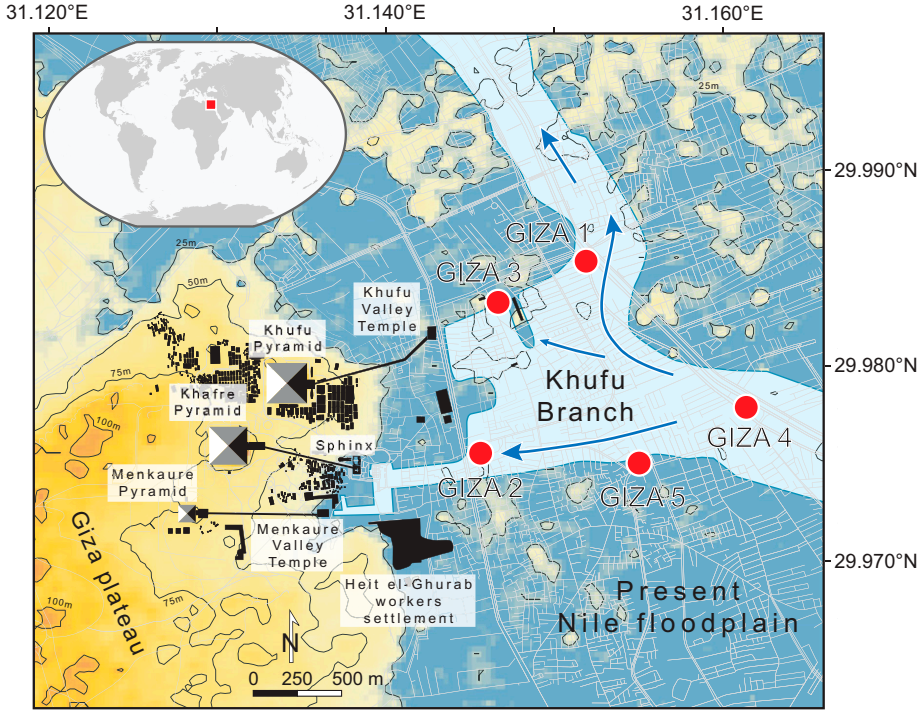


**Fig. 1.** Location of the cores on the Giza floodplain. The two cores used to reconstruct Holocene variations in Khufu-branch levels (cores G1 and G4) are located where the Khufu basin was connected to the Nile. The Giza Pyramid Complex currently lies >7 km from the present-day Nile branch. Harbor remains were previously found at the site of G3; the fluvial history derives from the work of Lehner (5, 6, 10, 11).

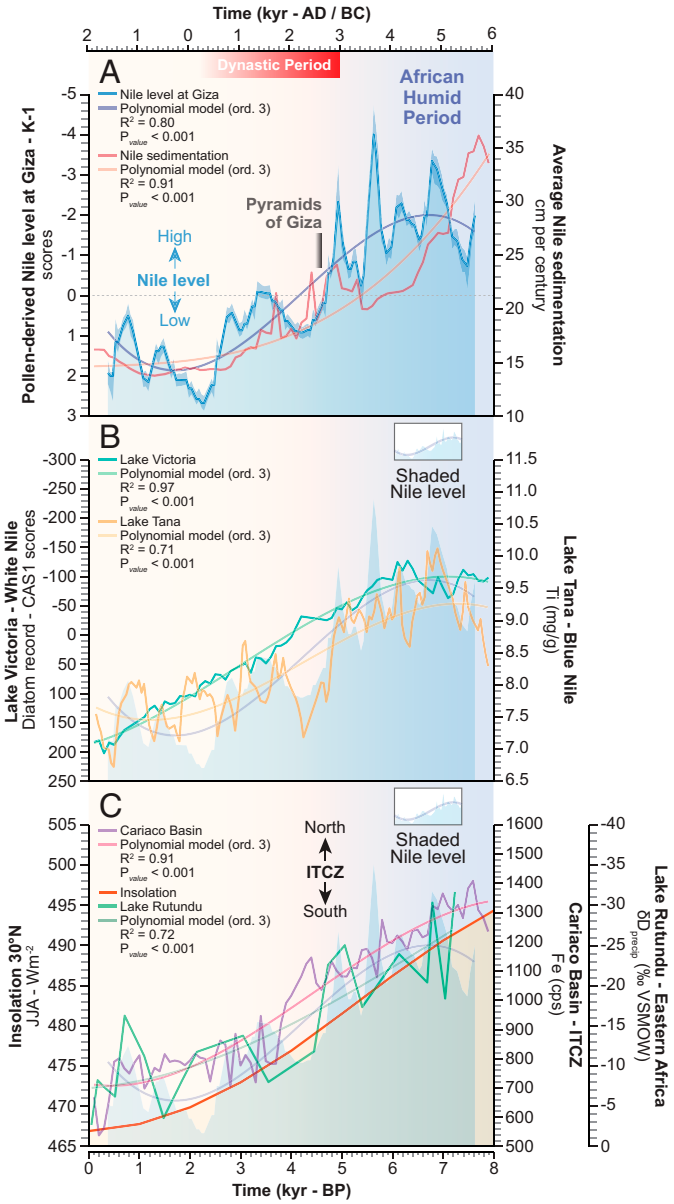


**Fig. 2.** Reconstructed Khufu-branch variations of the Nile during the last 8,000 y. (*A*) Pollen-derived Khufu-branch levels (K-1, blue line) expressed as Loess smoothing scores (with 2.5 and 97.5 percentiles) compared with Nile Delta sedimentation rates (red line) (19). Long-term trends are depicted by polynomial models (order 3, $P_{value} < 0.001$) (56). (*B*) Variations in Lake Victoria (White Nile) (22) and Lake Tana (Blue Nile) (21) reconstructed as a diatom record (red line) and Ti (mg/g; orange line). Long-term trends are depicted by polynomial models (order 3, $P_{value} < 0.001$) (56). The Khufu branch is represented by a shaded curve. (*C*) Summer insolation (56), migration of the ITCZ (25) shown as $Wm^{-2}$ (red line) and Fe (cps; purple line), and the Eastern African Monsoon shown as $\delta D_{precip}$ (‰ VSMOW) (24). Long-term trends are denoted by polynomial models (order 3, $P_{value} < 0.001$) (56). The Khufu branch is illustrated by a shaded curve. The background colors show the transition from the African Humid Period to the drying trend in Egypt.

Khufu branch (Fig. 2). The peak in the Khufu-branch level at 2950 ± 80 BCE (Fig. 2), while not documented in Lake Abiyata (Fig. 3), is recorded at Lake Rutundu, Lake Tana, and Lake Victoria, and on the Nile Delta (Figs. 2 and 3). Higher Khufu-branch levels at Giza are also in phase with higher levels in North African lakes (high and intermediate lakes; Fig. 3) (26). The most significant negative fluctuations in Khufu-branch levels during this period (~8000–5500 y ago) are correlated with volcanic forcing (correlation $R^2 = -0.30$; *SI Appendix*, Fig. S7) leading to diminished Nile summer flooding (27). Moreover, a drought episode recorded in Lake Tana at 5550 BCE, due to a southward shift in the monsoon front, is also documented by a drop in the Khufu-branch level at Giza 5550 ± 80 BCE (Fig. 2).

Following the African Humid Period, the Khufu branch manifests an important and permanent drop during the Early Dynastic Period (3000–2686 BCE) as reconstructed in the core K-1 (Fig. 4). This drop is correlated with a decline in human occupation in the Eastern Sahara (28) and a slight regression of sites in Upper and Lower Egypt (28). The first dynasties of Egypt played out during a major fall in the Nile level, as attested by the Khufu branch from 2970 ± 80 to 2690 ± 80 BCE, consistent with a hydrological shift at Lake Tana (Fig. 2)

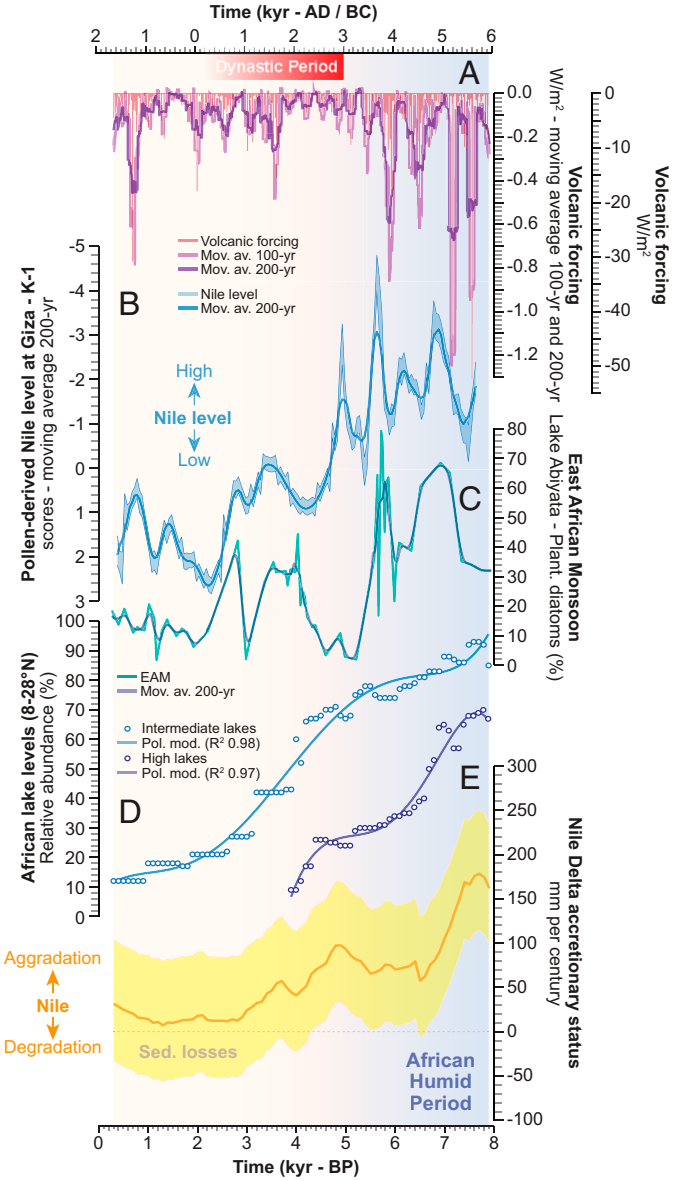


**Fig. 3.** Khufu-branch levels during the Holocene compared with volcanic forcing, East African Monsoon and North African lakes. (*A*) Volcanic forcing (57) expressed as $Wm^{-2}$ and shown as events (red line), 100-y (shaded light purple) and 200-y (shaded dark purple) moving averages. (*B*) Pollen-derived Khufu-branch levels (K-1, blue line) expressed as 2.5 and 97.5 percentiles, and as a 200-y moving average. (*C*) East African Monsoon (green line) reconstructed from planktonic diatoms recorded at Lake Abiyata, Ethiopia (23). The long-term trend is depicted by a 200-y moving average (shaded blue line). (*D*) North African lake levels (blue: intermediate and purple: high lakes) (26) shown as relative abundances. Long-term trends are illustrated by polynomial models (order 3, $P_{value} < 0.001$) (56). (*E*) Nile Delta accretionary status (19) shown in mm per century (orange) with the SD (yellow). The background colors show the transition from the African Humid Period to the drying trend in Egypt.

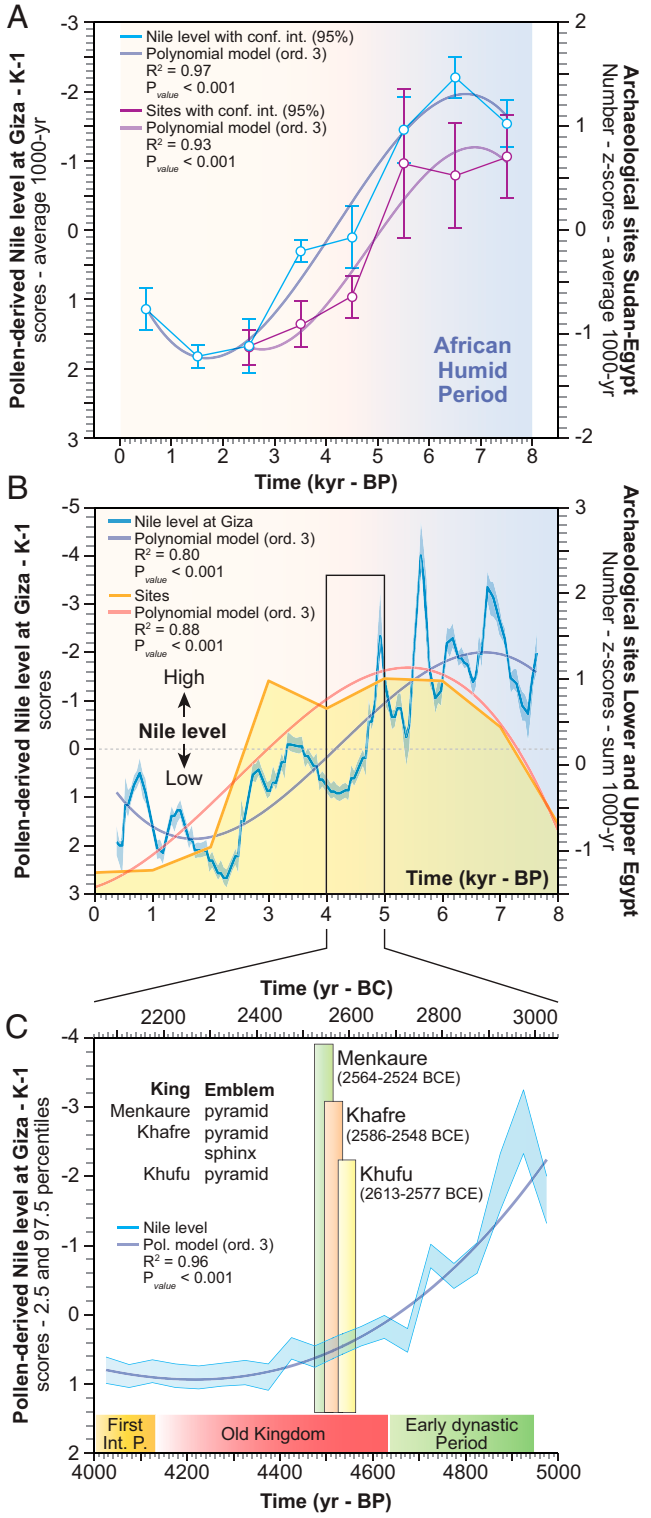


**Fig. 4.** Khufu-branch variations and North African archaeological sites. (*A*) Level of the Khufu branch (K-1, blue line) compared to the number of archaeological sites in Sudan and Egypt (light purple line) (28). Archaeological site numbers were transformed into z-scores. The two datasets are shown as 1,000-y averages (with a 95% confidence interval). Long-term trends are represented by polynomial models (order 3, $P_{value} < 0.001$) (56). (*B*) Level of the Khufu branch (blue line; Loess smoothing scores with 2.5 and 97.5 percentiles) compared to archaeological sites in Lower and Upper Egypt (orange line) (28). The number of archaeological sites is shown as a 1,000-y sum, transformed into z-scores. Long-term trends are illustrated by polynomial models (order 3, $P_{value} < 0.001$) (56). (*C*) Khufu-branch levels (2.5 and 97.5 percentiles) during the construction of the pyramids of kings Khufu, Khafre, and Menkaure (blue line). The long-term trend is represented by a polynomial model (order 3, $P_{value} < 0.001$) (56). The background colors show the transition from the African Humid Period to the aridification of Egypt (*A* and *B*).

and the onset of Nile Delta erosion due to decreasing sedimentation (19) (Fig. 3). This drop of the Khufu-branch level is part of long-term hydrological changes in Eastern Africa mainly triggered by orbitally driven insolation pacing as well as the variability of humid/arid periods (24, 29, 30). At Lake Abhe (Central Afar region), incursion of air moisture masses in the East African Rift System, caused by a high-pressure gradient between the Congo Air Boundary and the Indian Summer Monsoon air masses, resulted in heightened precipitation over Northeastern Africa (24). These conditions supported large waterbodies in the northern East African Rift System until ~2650 BCE (24). At Lake Tana, the persistence of a relatively high waterbody until at least 3000 BCE probably resulted from the same conditions, even if hydrological changes in the lake have occurred since 5850 BCE. This was caused by the southward migration of the ITCZ (31), inducing a reduction in rainfall over the Ethiopian Highlands, with the lowest level of the lake recorded at 2250 BCE (21). Nile flow (Fig. 2) followed the same trend.

During the first half of the Old Kingdom of Egypt (2686–2440 BCE; Fig. 4), the level of the Khufu branch of the Nile remained relatively constant, characterized by a level at ~40% of that reached during the African Humid Period (Fig. 2). This relatively stable phase is also recorded in North African lake levels (Fig. 3). From the third to the fifth dynasties, the Khufu branch clearly offered an environment conducive to the emergence and development of the pyramid construction site, helping builders to plan the transport of stone and materials by boat. As a consequence, the number of archaeological artifacts increased on the Giza plateau (32), particularly during the Fourth Dynasty. Between the reign of King Unas (accession date 2438–2397 BCE) (33) and the end of the Sixth Dynasty, the level (and probably the baseflow) of the Khufu branch attained its earliest low levels (Fig. 4). It has been suggested that a failure of the annual Nile flood caused severe famine episodes (34), leading to the first Intermediate Period (2160–2055 BCE). Regarding the Khufu branch at Giza, the first low point occurred at 2225 ± 80 BCE (Fig. 4), with a level that locally dropped by ~10% compared with the Great Pyramid stage. This low level resulted from a wider-scale climatic event (35, 36) that also affected North African lake levels (26).

The Khufu branch of the Nile rose again during the Middle Kingdom (2055–1650 BCE), stabilizing throughout the Second Intermediate Period (1650–1550 BCE), before declining again (after 1350 ± 80 BCE) during the New Kingdom (1550–1069 BCE; Fig. 2). After the reign of king Tutankhamun (accession date 1349–1338 BCE) (33), the level gradually declined and reached a low value at 1075–1025 ± 80 BCE, close to the level recorded at 2225 ± 80 BCE (Fig. 2). This shift, also widely recorded in Eastern Mediterranean paleoclimatology (37), is associated in Egypt with a weaker East African Monsoon, leading to a fall in level at Lake Tana (Fig. 2) and to a strong decline of North African lake levels (Fig. 3). In 1069 BCE, Egypt transitioned into the Third Intermediate Period, which lasted for 400 y (from the 21st to 24th the dynasties) (2). While the level of the Khufu branch again increased during the 22nd dynasty, from the reign of king Sheshonq I to the reign of king Osorkon IV, the end of the Third Intermediate Period and the Late Period recorded the most important drop in Nile levels at Giza. The level is the lowest documented during the last 8,000 y (Fig. 2). This pronounced fall is correlated with an increase in $\delta^{18}O$ values in teeth and bones from Egyptian mummies (38), suggesting a more arid environmental period (Fig. 5). A less intense East African Monsoon, low sedimentation and increased sediment losses on the Nile Delta all point to a dry phase that

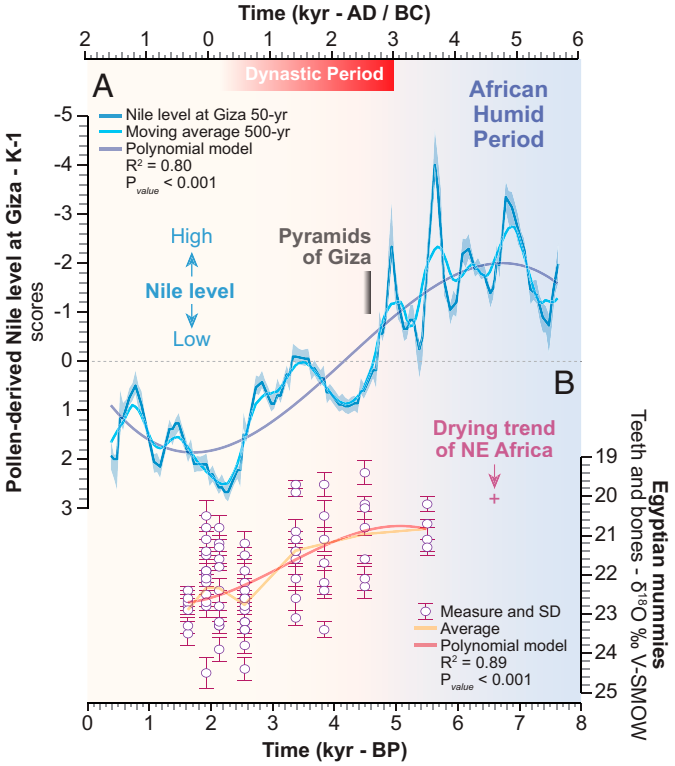


**Fig. 5.** Khufu-branch variations and Egyptian mummies geochemistry. (*A*) Pollen-derived Khufu-branch levels (K-1, blue line) expressed as Loess smoothing scores (with 2.5 and 97.5 percentiles). Long-term trends are depicted by a polynomial model (order 3, $P_{value} < 0.001$) (56). (*B*) $\delta^{18}O$ ‰ values (with SD) from Egyptian mummies (teeth and bones; light red) (38). The data are shown as averages and with a polynomial model (order 3, $P_{value} < 0.001$) (56) to highlight the long-term trend. The background colors show the transition from the African Humid Period to the aridification of Egypt.

lasted ∼600 y. According to Bunbury and Jeffreys (39), the Khufu branch was diminished to a small channel named "Maaty" by the Middle Kingdom. The level of the Khufu branch was extremely low during the New Kingdom and when Alexander the Great conquered Egypt, at the start of the Ptolemaic Period.

The chronology from the Early Dynastic to the Late Period has been widely debated. It derives from different sources, including textual evidence, astronomical observations and $^{14}C$ dating (2, 33, 40–43). Focusing on the Giza pyramids, the accession date of Khufu (Fig. 4) ranges from 2613 to 2577 BCE (1σ) according to the $^{14}C$-based chronology (33) while other sources place the onset of his reign at 2589 BCE (2), 2554 BCE (41), or 2480 ± 5 BCE based on astronomical observations (42). The same inaccuracy is noted for the reign of Khafre or Menkaure. The accession date of Khafre ranges from 2586 to 2548 BCE (1σ) (33) or is chronologically centered on 2558 BCE (2), 2522 BCE (41), or 2448 ± 5 BCE (42). The accession date of Menkaure ranges from 2564 to 2524 BCE (1σ) (33) with centers on 2532 BCE (2), 2489 BCE (41), or 2415 ± 10 BCE (42). The wide chronological ranges regarding the accession date of each king suggests that the use of the $^{14}C$ chronology (33) is preferable as less subject to interpretation. This is what was used in the present study.

Our 8,000-y reconstruction of Khufu-branch levels improves understanding of fluvial landscapes at the time of the construction of the Giza Pyramid Complex, and demonstrates that Old Kingdom engineers harnessed the fluvial environment—the Nile and its annual floods—to exploit the plateau area overlooking the floodplain for monumental construction. We suggest that these paleoclimate data can also be used as a template to understand the waterscapes bordering the earlier Saqqara and Dahshur pyramid complexes, also on the West Bank of the Nile, and respectively 16 km and 22 km south of Giza.

## Materials and Methods

**Cores and Chronology.** A total of five cores were drilled on the Giza floodplain (Fig. 1) in May 2019 under the auspices of the Egyptian National Research Institute of Astronomy and Geophysics. The cores G1 (890 cm depth; 29°59′04″N, 31°09′07″E; 18 m a.s.l.) and G4 (700 cm depth; 29°58′40″N, 31°09′39″E; 19 m a.s.l.) were selected to reconstruct the Khufu-branch levels because these two cores are located inside the supposed Khufu basin. The lithology of cores G1 and G4 is detailed in *SI Appendix*, Fig. S1. The chronology of the two cores is based on radiocarbon ($^{14}C$) dates of the total organic carbon fraction extracted from the sedimentary deposits. The cores were completely void of plant macrofossils. For dating purposes, we isolated only the most reliable organic-rich sediments, without any enrichment in old carbonates. Clam age-depth modeling (44, 45) was then used to build the age-models for G1 and G4 (*SI Appendix*, Fig. S2). Although based on a few reliable samples, the age models (G1 and G4) were supported by pottery sherds found in the sedimentary deposits. The samples are dated to the Predynastic and Early Dynastic-Old Kingdom periods by comparison with earlier studies at Giza (46) and Saqqara (47). The age-models are also corroborated by comparison with high-resolution sequences such as Lake Tana (21) (Fig. 2) or Lake Abiyata (23) (Fig. 3). All dates are expressed as Before Common Era (BCE) and Before Present (BP).

**Paleoecological Data.** We prepared a total of 109 samples for pollen analysis using standard procedures for clay deposits (48). Tablets of Lycopodium spores (∼20,848 spores/tablet) were added to each sample in order to estimate the pollen concentration. Pollen grains were counted under 400× and 1,000× magnification using an Olympus microscope. Atlases (49–52), books (48, 53, 54), as well as local reference slides were used for pollen identification. Pollen percentages are based on the terrestrial pollen sum, excluding the local helophytes (Alismataceae, Cyperaceae, *Sparganium*, and *Typha*) and spores of nonvascular cryptogams (ferns). Percentages of helophyte taxa were calculated using a sum that includes local freshwater plants and terrestrial vegetation. Percentages of ferns were calculated using a sum that includes local freshwater plants, terrestrial vegetation and ferns. Palynological slides were counted using a minimum sum of 100 grains. It has been shown that a pollen count of 70–150 grains is statistically significant for a 0.90 reliability (55). In arid and semiarid areas, pollen contributions from the vegetation cover are low, reducing the sample pollen content (55). The pollen data are here presented as concentration diagrams (number of pollen grains per $cm^{-3}$ of sediment; *SI Appendix*, Fig. S3). All the pollen slides are housed at the IMBE laboratory (France). The taxa were then clustered into pollen-derived vegetation groups (PdVs) based on their ecological affinities. Seven PdVs were defined: upland terrestrial herbs, Cyperaceae, helophytes (excluding the Cyperaceae), tropical Nilotic taxa, date palm-willow, cereals, and ferns (*SI Appendix*, Table S1).

**Composite Sequence.** The two cores were merged, based on the $^{14}C$ chronology, to create a single composite sequence, termed K-1 (for Khufu-1). The paleoecological dataset for this sequence is based on the average (G1 and G4) of each PdV for each sample (*SI Appendix*, Fig. S6).

**Reconstruction of Holocene Variations in the Level of the Nile's Khufu Branch.** All the PdV time series from K-1(expressed as percentages) were regularly interpolated to a 50-y interval, consistent with the average chronological resolution of cores G1 and G4. The time series were then converted into z-scores and the results used as a data matrix for cluster analyses (with paired group as the algorithm and correlation as the distance measure) to individualize the PdV located inside and outside the Nile floodplain (*SI Appendix*, Fig. S4). The link between these two groups was tested, ranking the Nile floodplain vegetation scores in ascending order and retaining the associated vegetation scores from beyond the Nile floodplain (*SI Appendix*, Fig. S5). The two datasets are depicted with their confidence interval (95%). The two groups were also cross-correlated to ascertain the best temporal match. The correlation coefficient ($R^2$) is then given, focusing on the $Lag_0$ value (with +0.50 and −0.50 as significant thresholds). A principal component analysis (PCA) was subsequently performed to test

the ordination of samples by assessing major changes in the PdV-scores (56). The first axis (PCA-Axis 1), which carries the maximum variance, has been extracted (56). The PdVs influenced by the Nile floodplain are loaded by the negative scores of PCA-Axis 1 while the PdVs located outside the Nile influence are loaded by the positive scores (*SI Appendix*, Fig. S4). We then transformed the PCA-Axis1 scores using a Loess smoothing (with a LOWESS algorithm) and performed a bootstrap to estimate a 95% confidence band based on 1,000 random replicates (56). The Loess curve and the 95% confidence band were used as a proxy for the Khufu-branch level (Fig. 2) (56).

**Long-Term Trends.** The long-term trends were calculated using polynomial models (order 3, $P_{value} < 0.001$) (56) and a moving average function (100-y and 200-y).

**Other Proxies.** We compared Holocene variations in the level of the Khufu branch using various high-resolution datasets including: the Nile Delta (19, 20), Lake Tana (21), Lake Victoria (22), Lake Rutundu (24), the Cariaco basin (25), summer insolation (57), volcanic forcing (27, 58), Lake Abiyata (23), African lake levels (26), archaeological sites in Upper and Lower Egypt (28), and Egyptian mummies (38). To probe the link between these time series and variations in the Khufu branch, cross-correlations ($P = 0.05$) were calculated (*SI Appendix*, Fig. S7). Positive and negative correlation coefficients are considered, focusing on the $Lag_0$ value.

**Data from Archaeological Sites in Sudan and Egypt.** The number of sites in Sudan and Egypt (29) was converted into a moving 1,000-y sum and transformed into z-scores (Fig. 4). The Khufu branch was converted into a moving 1,000-y average for comparative purposes. The two datasets are depicted with their confidence interval (95%).

**Software.** All the statistical analyses were performed using R 4.1.0, Past 4.03, and XL-Stat[2019] software.

**Data Availability.** All study data are included in the article and/or *SI Appendix*.

**ACKNOWLEDGMENTS.** Drilling permission was obtained with the help of the National Research Institute of Astronomy and Geophysics (NRIAG, Helwan, Egypt). This research project was financially supported by National Natural Science Foundation of China (41620104004). This study received financial supports from the CEREGE laboratory (APIC Research project), the MITI-CNRS "Evénements rares" program (AQUASANMARCO project), the ARKAIA Institute (GIZA project), the MSHE-Université de Franche-Comté (GIZAPORT project), the Excellence Initiative of Aix-Marseille University, and the A*MIDEX, a French "Investissements d'Avenir" programme.

Author affiliations: [a]Aix Marseille Université, CNRS, IRD, INRA, Collège de France, CEREGE, 13545 Aix-en-Provence Cedex 04, France; [b]Europôle méditerranéen de l'Arbois, Institut Méditerranéen de Biodiversité et d'Ecologie - IMBE (Aix Marseille Univ, Avignon Université, CNRS, IRD), 13545 Aix-en-Provence Cedex 04, France; [c]TRACES, UMR 5608 CNRS, Université Toulouse Jean Jaurès, Maison de la Recherche, 31058 Toulouse Cedex 9, France; [d]Département de Biologie et Géosciences, Université Paul Sabatier - Toulouse 3, 31062 Toulouse Cedex 9, France; [e]CNRS, ThéMA, Université de Franche-Comté, UMR 6049, MSHE Ledoux, 25030 Besançon, France; [f]Department of Geography and GIS, Faculty of Arts, Ain Shams University, 11516 Ain Shams Cairo, Egypt; [g]SKLEC-State Key Laboratory of Estuarine and Coastal Research, East China Normal University ECNU, Shanghai 200062, China; [h]National Research Institute of Astronomy and Geophysics, 11421 Helwan, Egypt; and [i]EPHE-Section des Sciences Historiques et Philologiques, AOROC, UMR 8546 - Archéologie et Philologie d'Orient et d'Occident, CNRS/PSL, École Normale Supérieure, 75230 Paris Cedex 5, France

1. M. A. J. Williams, *The Nile Basin: Quaternary Geology, Geomorphology and Prehistoric Environments* (Cambridge University Press, Cambridge, 2019).
2. I. Shaw, Ed., *The Oxford History of Ancient Egypt* (Oxford University Press) 2000).
3. B. Bell, The oldest records of the Nile floods. *Geogr. J.* **136**, 569–573 (1970).
4. F. A. Hassan, Historical Nile floods and their implications for climatic change. *Science* **212**, 1142–1145 (1981).
5. M. Lehner, On the waterfront: Canals and harbors in the time of Giza pyramid-building. *Aearagram* **15**, 13–23 (2014).
6. M. Lehner, "Lake Khufu: on the waterfront at Giza – modelling water transport infrastructure in Dynasty IV" in *Profane Landscapes, Sacred Spaces*, M. Bárta, J. Janák, Eds. (Equinox Publishing, Sheffield, United Kingdom 2020), pp. 191–292.
7. K. W. Butzer *et al.*, Urban geoarchaeology and environmental history at the Lost City of the Pyramids, Giza: synthesis and review. *J. Archaeol. Sci.* **40**, 3340–3366 (2013).
8. J. P. Cooper, *The Medieval Nile* (The American University in Cairo Press, 2014).
9. P. Tallet, *Les Papyrus de la Mer Rouge I: 'Journal de Merer' (Papyrus Jarf A et B)* (Institut Français D'archéologie Orientale, 2017).
10. M. Lehner, W. Wetterstrom, *Giza Reports, I. Project History, Survey, Ceramics, and Main Street and Gallery. III.4 Operations* (Ancient Egypt Research Associates, 2007).
11. M. Lehner, "A. Tavares" in *Cities and Urbanism in Ancient Egypt*, M. Bietak, Ed. (Österreichische Akademie der Wissenschaften, 2010), pp. 171–216.
12. P. Tallet, Note d'information: Les Papyrus de la Mer Rouge (Ouadi el-Jarf, Golfe de Suez). *CRAI* **2**, 1015–1024 (2013).
13. P. Tallet, G. Marouard, The harbor facilities of king Khufu on the Red Sea shore: the Wadi al-Jarf/Tell Ras Budran system *J. Am. Res. Cent. Egypt* **52**, 135–177 (2016).
14. T. Shanahan *et al.*, The time-transgressive termination of the African Humid Period. *Nat. Geosci.* **8**, 140–144 (2015).
15. J. E. Tierney, F. S. R. Pausata, P. B. deMenocal, Rainfall regimes of the Green Sahara. *Sci. Adv.* **3**, e1601503 (2017).
16. M. Jones, A new Old Kingdom settlement near Ausim: Report of the archaeological discoveries made in the Barakat Drain Improvements Project. *Mitt. Dtsch. Archaeol. Inst. Abt. Kairo* **51**, 85–98 (1995).
17. A. El-Sanussi, M. Jones, A site of the Maadi culture near the Giza pyramids. *Mitt. Dtsch. Archaeol. Inst. Abt. Kairo* **53**, 241–253 (1997).
18. P. B. DeMenocal, End of the African Humid period. *Nat. Geosci.* **8**, 86–87 (2015).
19. N. Marriner *et al.*, Nile delta subsidence: Quantifiable links with Holocene compaction and changes in sediment supply? *Geology* **40**, 1083–1086 (2012).
20. N. Marriner *et al.*, ITCZ and ENSO-like modulation of Nile delta hydro-geomorphology during the Holocene. *Quat. Sci. Rev.* **45**, 73–84 (2012).
21. M. H. Marshall *et al.*, Late Pleistocene and Holocene drought events at Lake Tana, the source of the Blue Nile. *Global Planet. Change* **78**, 147–161 (2011).
22. J. C. Stager, B. F. Cumming, L. D. Meeker, A 10,000-year high-resolution diatom record from Pilkington Bay, Lake Victoria, East Africa. *Quat. Res.* **59**, 172–181 (2003).
23. F. Chalié, F. Gasse, Late Glacial-Holocene diatom record of water chemistry and lake level change from the tropical East African Rift Lake Abiyata (Ethiopia). *Palaeogeogr. Palaeoclimatol. Palaeoecol.* **187**, 259–283 (2002).
24. C. Mologni *et al.*, Holocene East African monsoonal variations recorded in wave-dominated clastic paleo-shorelines of Lake Abhe, Central Afar region (Ethiopia and Djibouti). *Geomorphology* **391**, 107896 (2021).
25. T. Schneider, T. Bischoff, G. H. Haug, Migrations and dynamics of the intertropical convergence zone. *Nature* **513**, 45–53 (2014).
26. J. E. Tierney, S. C. Lewis, B. I. Cook, A. N. LeGrande, G. A. Schmidt, Model, proxy and isotopic perspectives on the East African Humid Period. *Earth Planet. Sci. Lett.* **307**, 103–112 (2011).
27. J. G. Manning *et al.*, Volcanic suppression of Nile summer flooding triggers revolt and constrains interstate conflict in ancient Egypt. *Nat. Commun.* **8**, 900 (2017).
28. R. Kuper, S. Kröpelin, Climate-controlled Holocene occupation in the Sahara: Motor of Africa's evolution. *Science* **313**, 803–807 (2006).
29. L. Bastian *et al.*, Co-variations of climate and silicate weathering in the Nile Basin during the Late Pleistocene. *Quat. Sci. Rev.* **264**, 107012 (2021).
30. S. Garelick, J. M. Russell, S. Dee, D. Verschuren, D. O. Olago, Atmospheric controls on precipitation isotopes and hydroclimate in high-elevation regions in Eastern Africa since the Last Glacial Maximum. *Earth Planet. Sci. Lett.* **567**, 116984 (2021).
31. P. deMenocal *et al.*, Abrupt onset and termination of the African Humid Period: Rapid climate responses to gradual insolation forcing. *Quat. Sci. Rev.* **19**, 347–361 (2000).
32. G. Lucarini *et al.*, The MedAfriCarbon radiocarbon database and web application. Archaeological dynamics in Mediterranean Africa, ca. 9600-700 BC. *JOAD* **8**, 1 (2020).
33. C. Bronk Ramsey *et al.*, Radiocarbon-based chronology for dynastic Egypt. *Science* **328**, 1554–1557 (2010).
34. J. D. Stanley, M. D. Krom, R. A. Cliff, J. C. Woodward, Nile flow failure at the end of the Old Kingdom, Egypt: Strontium isotopic and petrologic evidence. *Geoarchaeology* **18**, 395–402 (2003).
35. H. Weiss, Ed., *Megadrought and Collapse: From Early Agriculture to Angkor* (Oxford University Press, 2017).
36. D. Kaniewski *et al.*, The 4.2 ka BP event in the Levant. *Clim. Past* **14**, 1529–1542 (2018).
37. D. Kaniewski *et al.*, Drought and societal collapse 3200 years ago in the Eastern Mediterranean: A review. *Wiley Interdiscip. Rev. Clim. Change* **6**, 369–382 (2015).
38. A. Touzeau *et al.*, Egyptian mummies record increasing aridity in the Nile valley from 5500 to 1500 yr before present. *Earth Planet. Sci. Lett.* **375**, 92–100 (2013).
39. J. Bunbury, D. Jeffreys, Real and literary landscapes in ancient Egypt. *Camb. Archaeol. J.* **21**, 65–76 (2011).
40. K. A. Kitchen, The chronology of Ancient Egypt. *World Archaeol.* **23**, 201–208 (1991).
41. J. von Beckerath, *Chronologie des Pharonischen Ägypten* (von Zabern, 1997).
42. K. Spence, Ancient Egyptian chronology and the astronomical orientation of pyramids. *Nature* **408**, 320–324 (2000).
43. R. Gautschy *et al.*, A new astronomically based chronological model for the Egyptian Old Kingdom. *J. Egypt. Hist.* **10**, 69–108 (2017).
44. M. Blaauw, Methods and code for 'classical' age-modelling of radiocarbon sequences. *Quat. Geochronol.* **5**, 512–518 (2010).
45. M. Blaauw, J. A. Christen, D. Mauquoy, J. van der Plicht, K. D. Bennett, Testing the timing of radiocarbon-dated events between proxy archives. *Holocene* **17**, 283–288 (2007).
46. K. Sowada, M. Ownby, A. Wodzińska, The petrography of imported Levantine combed vessels from early Old Kingdom Giza. *Levant* **52**, 197–214 (2020).
47. M. A. Hamdan *et al.*, Ancient Egyptian pottery from the subsurface floodplain of the Saqqara-Memphis area: Its mineralogical and geochemical implications. *Archaeometry* **56**, 987–1008 (2014).
48. K. Faegri, I. Iversen, *Textbook of Pollen Analysis* (Wiley, London), ed. 4, 1989).
49. R. Bonnefille, G. Riollet, *Pollens des Savanes d'Afrique Orientale* (Éditions du Centre National de la Recherche Scientifique, Paris, 1980).
50. M. Reille, *Pollen et Spores d'Europe et d'Afrique du Nord* (Louis-Jean, 1992).
51. M. Reille, *Pollen et Spores d'Europe et d'Afrique du Nord. Sup. I* (Empora, 1995).
52. M. Reille, *Pollen et Spores d'Europe et d'Afrique du Nord. Sup. II* (Louis-Jean, 1998).
53. P. D. Moore, J. A. Webb, M. E. Collinson, *Pollen Analysis* (Blackwell Scientific Publications, ed. 2, 1991).
54. W. Punt, S. Blackmore, *The Northwest European Pollen Flora* (Elsevier, Amsterdam, 1991), vol. VI.
55. M. Djamali, K. Cilleros, Statistically significant minimum pollen count in Quaternary pollen analysis; the case of pollen-rich lake sediments. *Rev. Palaeobot. Palynol.* **275**, 104156 (2020).
56. D. Kaniewski *et al.*, Northern Adriatic environmental changes since 500 AD reconstructed at Aquileia (Italy). *Quat. Sci. Rev.* **287**, 107565 (2022).
57. J. Laskar, A. Fienga, M. Gastineau, H. Manche, La2010: A new orbital solution for the long-term motion of the Earth. *Astron. Astrophys.* **532**, A89 (2011).
58. T. Kobashi *et al.*, Volcanic influence on centennial to millennial Holocene Greenland temperature change. *Sci. Rep.* **7**, 1441 (2017).